SUPPLEMENTAL FIGURES

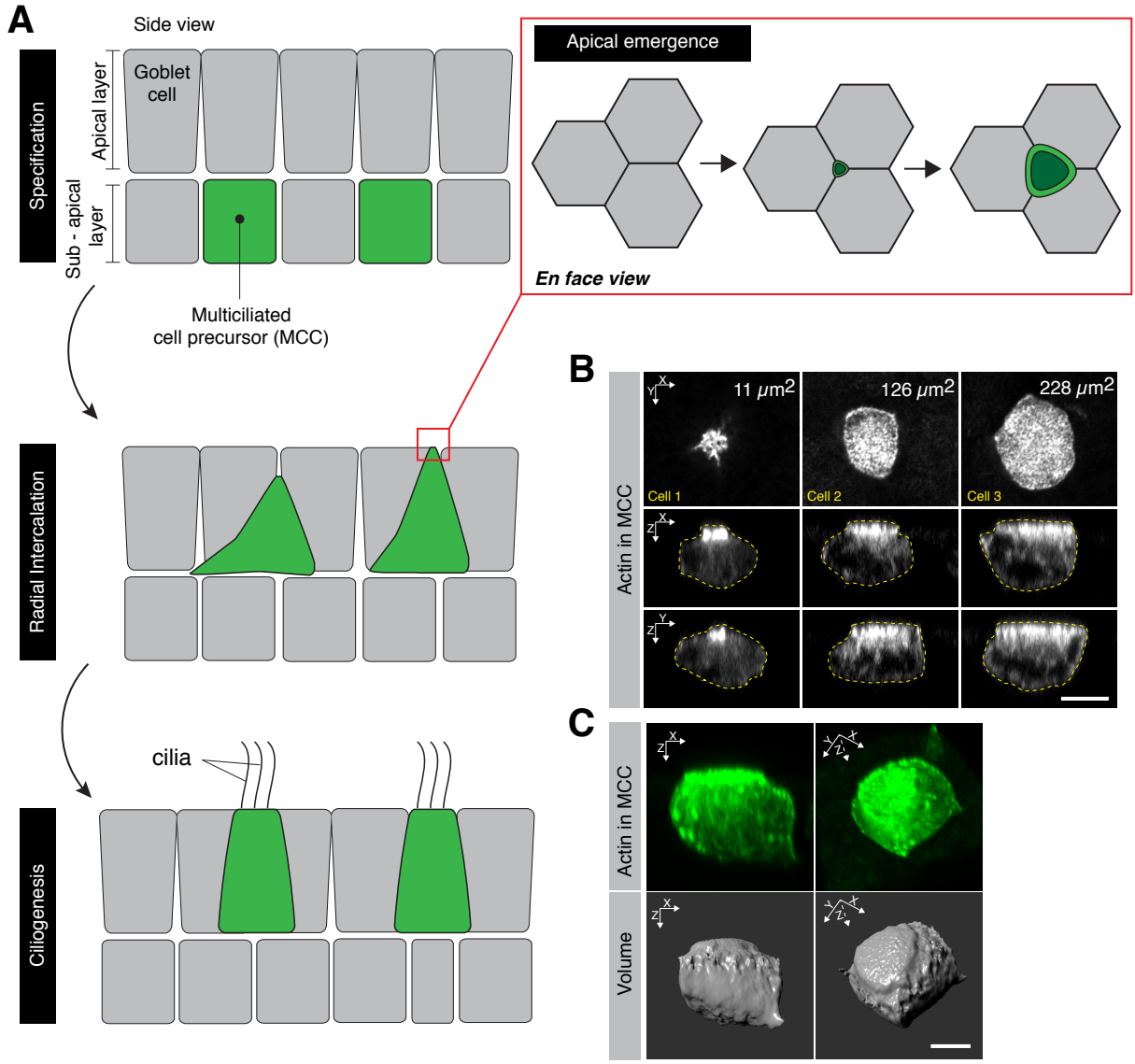

Figure S1. Related to Figure 1. Apical emergence is specific to the apical domain of MCCs. (A) Three phases of MCCs formation. After specification from basally-positioned progenitors, nascent MCCs (green) radially intercalate, moving apically and inserting at multicellular junctions. Following insertion, the apical surface of MCC precursor expands (apical emergence; red box at top right). Only after apical emergence is completed, cilia start to grow from the apical domain of MCCs. **(B)** Apical (top) and orthogonal (middle, bottom) views of apically emerging MCCs (visualized by α-tubulin UtrCH-GFP after immunostaining against GFP and clearing of embryos) at different stages of apical emergence. Scale bar, 10 µm. **(C)** Volume rendering of MCC expressing UtrCH-GFP in cleared embryos.

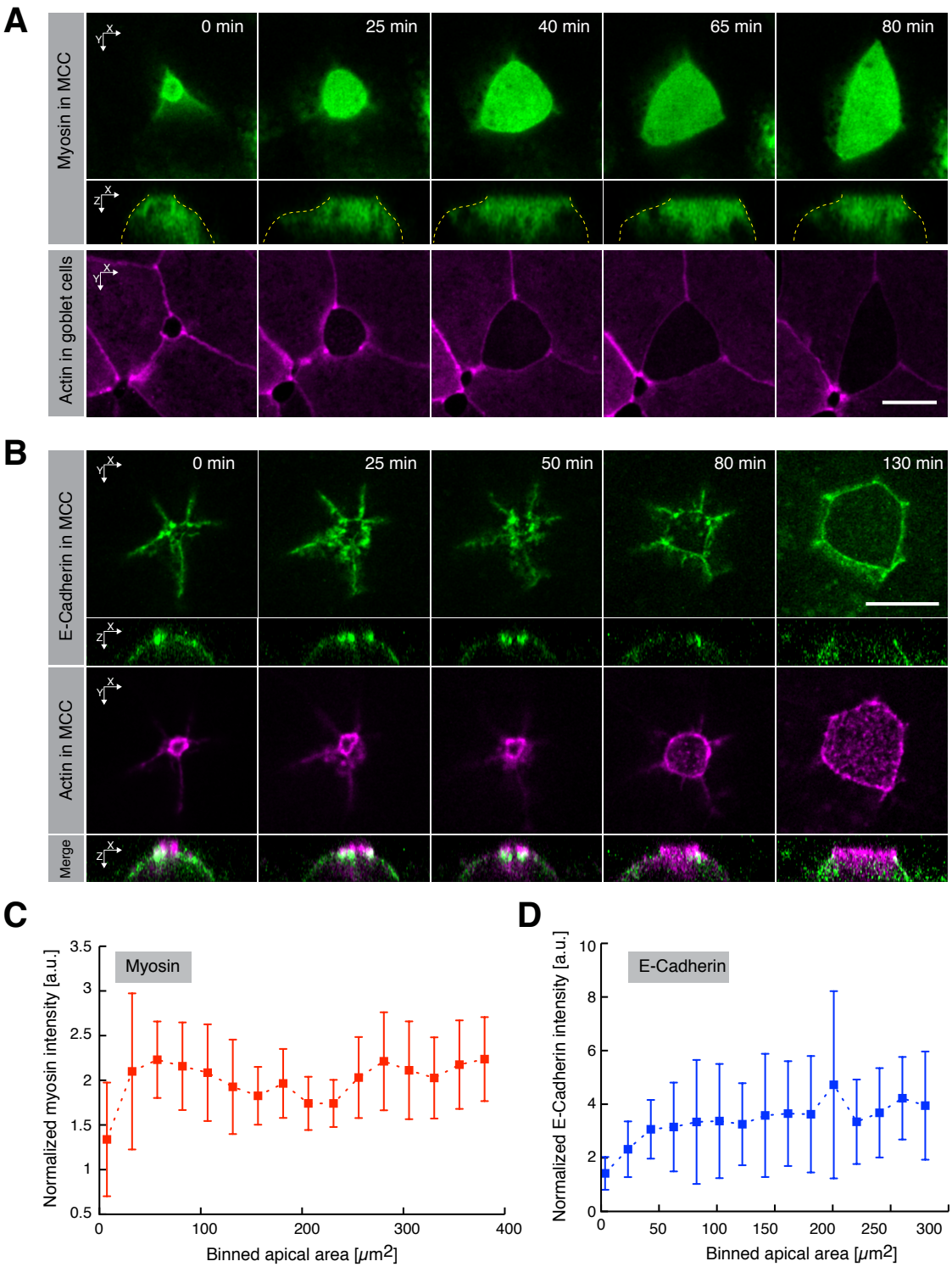

Figure S2. Related to Figure 1. Myosin and E-Cadherin dynamics during MCC apical emergence. (A) Image sequence of apically expanding MCC expressing myosin marker - myl12b, green, under MCC specific α-tubulin promoter; goblet cells visualized by expression of UtrCH-RFP (magenta) under goblet specific nectin promoter; top

and bottom panels - *en face* views, middle panel - orthogonal views. **(B)** Image sequence of apically expanding MCC expressing adherent junctions marker - E-Cadherin, green, under MCC specific α-tubulin promoter; actin in the same cell was visualized by expression of UtrCH-RFP (magenta) under MCC specific α-tubulin promoter; top panels - *en face* views, bottom panels - orthogonal views. Scale bar, 10 µm. **(C)** Normalized cortical myosin intensities (ratio of cortical to medial myosin within the apical domain) during MCCs apical emergence. Data represent mean and standard deviation from n=5 cells. **(D)** Normalized cortical E-Cadherin intensities (ratio of cortical to medial E-Cadherin within the apical domain) during MCCs apical emergence. Data represent mean and standard deviation from n=5 cells.

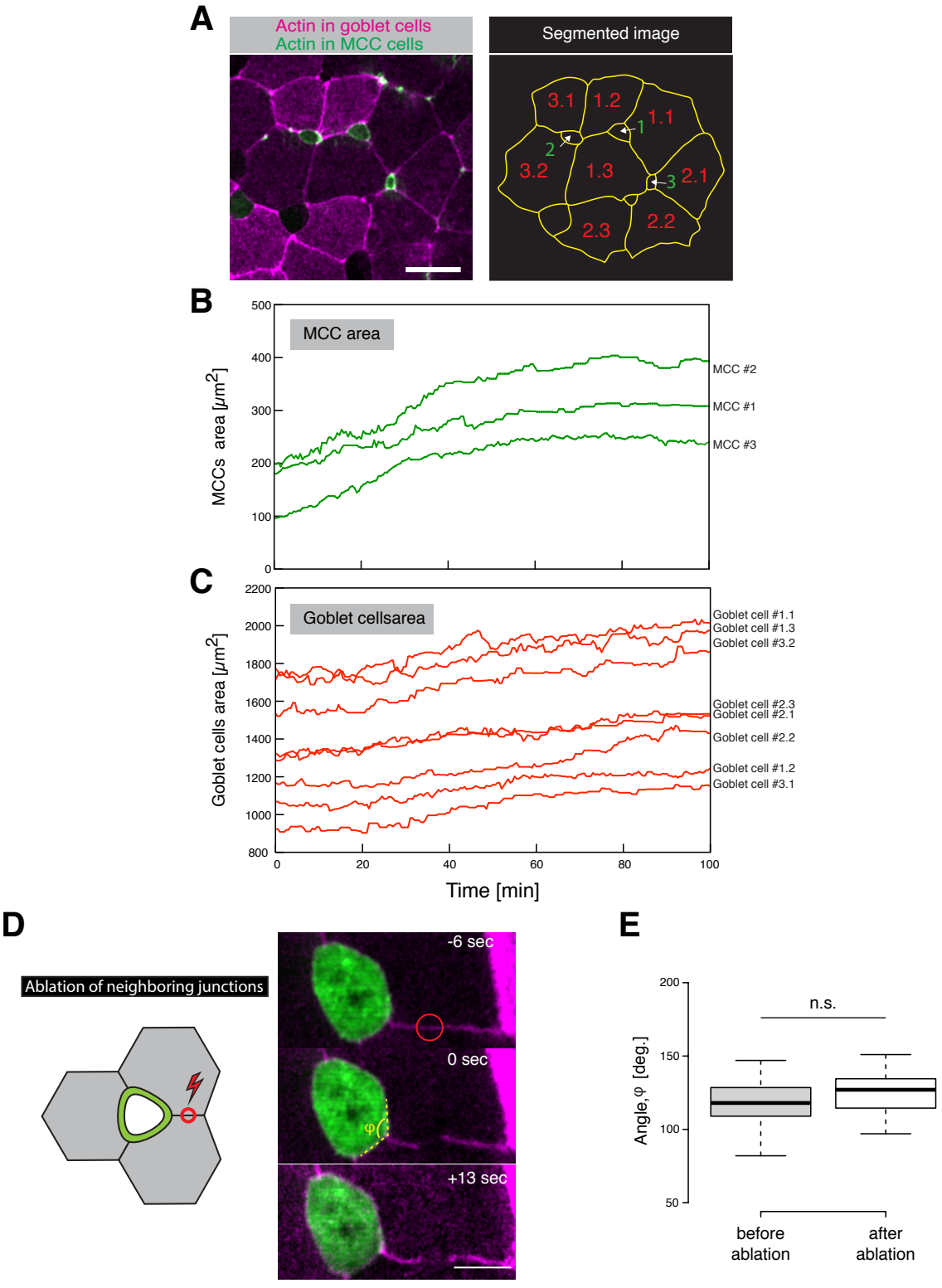
A
Actin in goblet cells
Actin in MCC cells
Segmented image
3.1
1.2
1.1
1
2
3.2
1.3
3
2.1
2.3
2.2
B
MCC area
MCCs area [μm2]
500
400
300
200
100
0
MCC #2
MCC #1
MCC #3
C
Goblet cellsarea
Goblet cells area [μm2]
2200
2000
1800
1600
1400
1200
1000
800
0
20
40
60
80
100
Time [min]
Goblet cell #1.1
Goblet cell #1.3
Goblet cell #3.2
Goblet cell #2.3
Goblet cell #2.1
Goblet cell #2.2
Goblet cell #1.2
Goblet cell #3.1
D
Ablation of neighboring junctions
-6 sec
0 sec
φ
+13 sec
E
Angle, φ [deg.]
200
150
100
50
n.s.
before ablation
after ablation

Figure S3. Related to Figure 2. Goblet cells do not pull on MCCs. (A) Schematic of MCCs and goblet cells segmentation. **(B)** MCCs and goblet cells **(C)** area change during apical emergence. Note that goblet cells do not decrease their apical area but rather marginally increase it, which strongly suggest that there is no constriction of goblet cells that might contribute to apical emergence. **(D)** Left: schematic of laser ablation of MCC neighboring junction. Red circle indicates ablation region. Right: ablation of MCC neighboring junction (visualized with nectin UtrCH-RFP, magenta), does not collapse MCC apical domain (visualized with α-tubulin UtrCH-GFP, green). 0 sec indicates time of ablation. **(E)** Quantification of the angle (φ, see S3D) change before and 10 seconds after ablation. Note that there is no dramatic collapse of a tricellular junction (measured by φ angle) nor change of a curvature upon laser ablation, which would be expected if junctional pulling would massively contribute to apical expansion. Boxes extend from the 25th to 75th percentiles, with a line at the median. P values, Mann-Whitney U test (number of cells, n=12 from 12 embryos), n.s. - not significant. Scale bar, 10 µm.

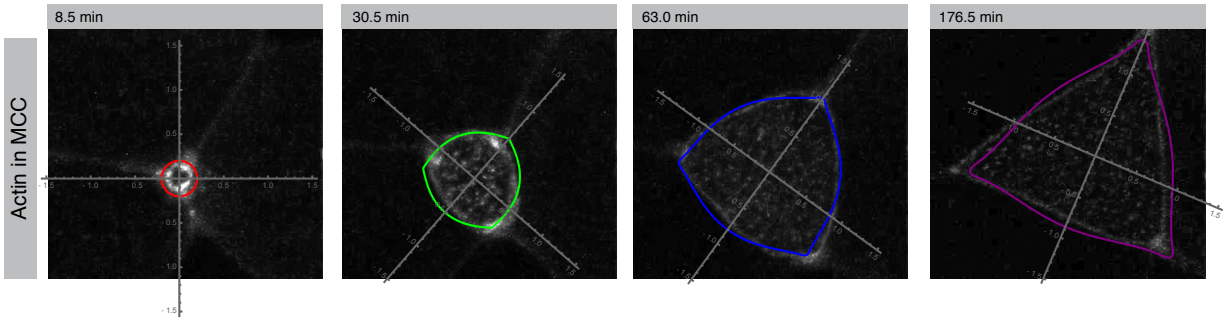

Figure S4. Related to Figure 3. Theoretical model of the apical expansion process is in good agreement with experimental data. The shape changes of the apical domain predicted by the theoretical model are overlaid on time-lapse images to highlight the similarity between the model and the experimental data.

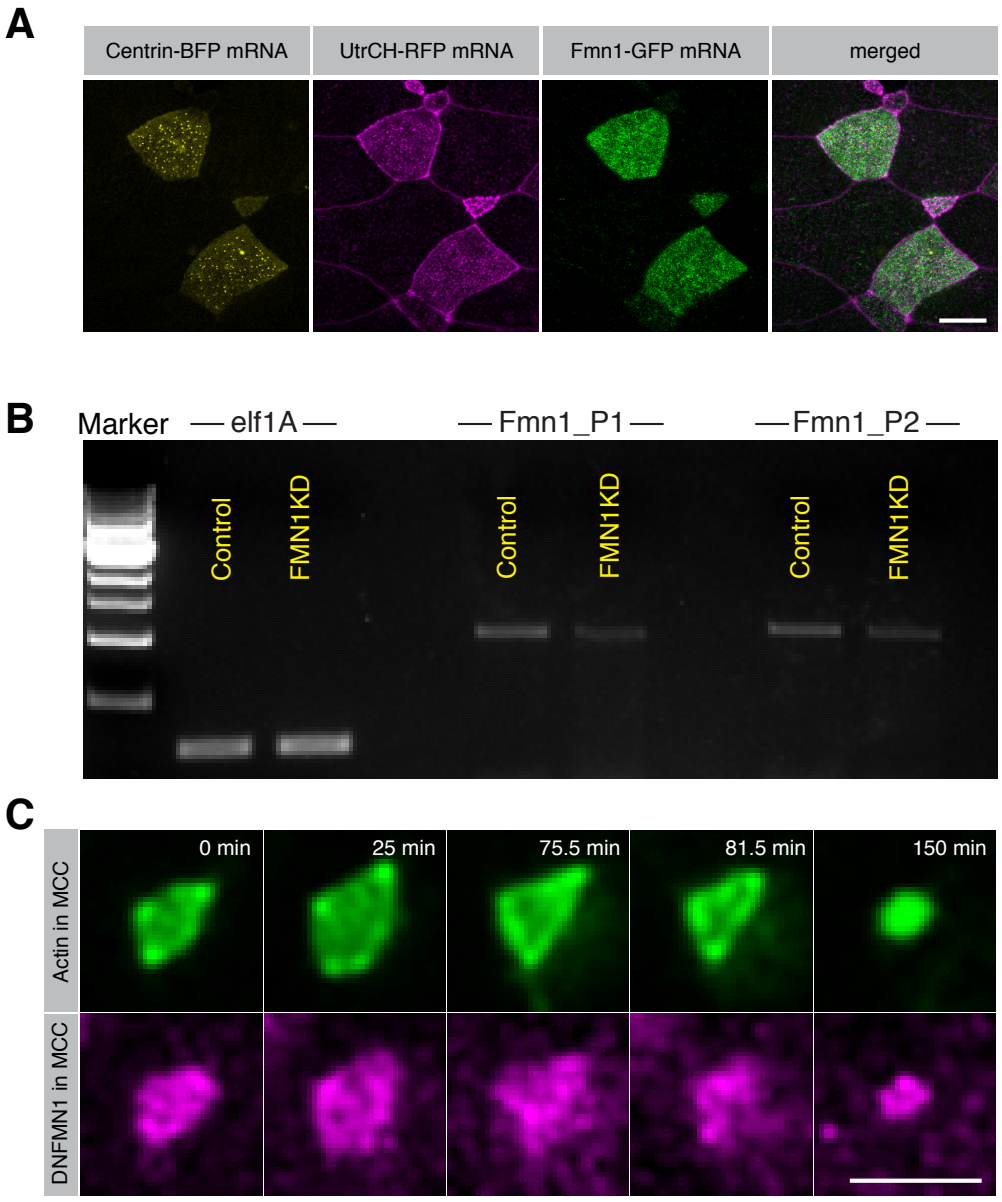

Figure S5. Related to Figure 5. Formin 1 regulates apical expansion of MCCs. (A) FMN1 (visualized by FMN1-GFP mRNA) is strongly expressed in MCCs. **(B)** Expression levels of FMN1 in controls and FMN1 KD. FMN1 levels are reduced in morphants as assessed by two different RT-PCR reactions. **(C)** Image sequence of apically collapsing MCC (visualized by α-tubulin UtrCH-GFP, green) expressing dominant negative version of FMN1 (DNFMN1) tagged with RFP, magenta). Scale bar, 10 µm.

Conditions	% of collapsing / overshooting cells	*n =
Controls	0 / 0	35
FMN1 KD	30.6 / 20.4	49
FMN1 Dominant negative	35.8 / 18.8	53
SMIFH2	44 / 0	40
Nectin CARhoA	0 / 13	23
Nectin DNRhoA	0 / 13	23

* From n > 5 embryos

Table S1. Related to Figure 5 and Figure 6. Frequency of apical domain collapses in various experimental conditions.

SUPPLEMENTAL MOVIE LEGENDS

Movie S1. Related to Figure 1 and Figure 3. Apical emergence of nascent multiciliated cells (MCCs) within *Xenopus laevis* epithelium. Time-lapse movie of an apically expanding MCC (visualized by α-tubulin UtrCH-GFP, green), within goblet cells (visualized by nectin UtrCH-RFP, magenta). Scale bar, 10 µm.

Movie S2. Related to Figure 1. Apical emergence is selectively driven in the apical region of nascent multiciliated cells (MCCs). Time-lapse movie of orthogonal projections of apically expanding MCC (visualized by α-tubulin UtrCH-GFP, green). Scale bar, 10 µm.

Movie S3. Related to Figure 4. Formation of medial apical actin of MCCs highly correlates with apical domain expansion dynamics. Time-lapse movie of automatically segmented cortical (between green and red lines) and medial (within the red line) regions within apically emerging MCC (visualized by α-tubulin UtrCH-GFP). Scale bar, 10 µm.

Movie S4. Related to Figure 5. FMN1 downregulation leads to 'overshooting' phenotype. Time-lapse movie of MCC (visualized by α-tubulin UtrCH-GFP, green) expressing dominant negative version of FMN1 (DNFMN1) undergoing multiple rounds of expansion and constriction of apical domain. Scale bar, 10 µm.

Movie S5. Related to Figure 5. FMN1 regulates apical emergence of MCCs. Time-lapse movie of apically constricting MCC (visualized by α-tubulin UtrCH-GFP, green) upon mosaic co-injection of FMN1 MO with mRNA of UtrCH-RFP, magenta. FMN1 MO is targeted to MCC as indicated by UtrCH-RFP expression. Scale bar, 10 µm.

Movie S6. Related to Figure 6. Neighboring cells resist apical expansion of MCCs. Time-lapse movie of apically expanding MCC (visualized by α-tubulin UtrCH-GFP, green) within goblet cells expressing constitutively active RhoA (CARhoA) (visualized by nectin CARhoA-RFP, magenta). Scale bar, 10 µm.

SUPPLEMENTAL EXPERIMENTAL PROCEDURE

***Xenopus* embryo manipulations**

Xenopus laevis adult females were ovulated by injection of human chorionic gonadotropin. The following day, eggs were squeezed, fertilized in vitro and dejellied in 3% cysteine (pH 7.9). Fertilized embryos were washed and subsequently reared in 1/3X Marc's Modified Ringer's (MMR) solution. For microinjections, embryos were placed in a solution of 2% Ficoll in 1/3X MMR and injected using glass capillary pulled needle, forceps, and an Oxford universal micromanipulator.

Cloning, plasmids, morpholinos, and drugs treatment

To determine the effectiveness of FMN1MO, embryos were injected at the top part of all 4 cells at four-cell stage with control solution or FMN1 MO solution. Animal caps were collected at stage 9 and were used for RNA extraction at stage 18. cDNAs were prepared using the Superscript kit (Invitrogen) and PCR was performed using specific primers. Input control primers:

EF1a-F: CAGATTGGTGCTGGATATGC,
Ef1a-R: ACTGCCTTGATGACTCCTAG.
FMN1 primer set1:
FMN1-E1F: TAAATTGCAGGACATTAGCACTTGTGTGC,
FMN1-E3R: TGCTTCAGTGTATTTCAGACCCACTTTTTC.
FMN1 primer set 2:
FMN1-E1F: TAAATTGCAGGACATTAGCACTTGTGTGC,
FMN1-E4R: CTTCAGCTCCTCTGTCTCATCCTTG.

Morpholino oligonucleotide, mRNA, and plasmids injections

FMN1-MO was injected at 10 ng per blastomere. The amounts of injected mRNAs were as follows: RFP-UtrCH [60pg (per blastomer)], GFP-FMN1 [300pg (per blastomere)]. The amounts of injected plasmids were as follows: α-tubulin GFP-UtrCH [25pg], α-tubulin RFP-UtrCH [25pg], α-tubulin GFP-DNFMN1 [25pg], nectin GFP-UtrCH [25pg], nectin RFP-UtrCH [25pg], nectin DNRhoA-RFP [30pg], nectin CARhoA-RFP [30pg].

Laser ablations

Local laser ablation experiments were performed with pulsed laser (Photonics Instruments) tuned to 435nm using 15 repetitions pulses at 20Hz. Time-lapse imaging was performed throughout ablation process using a Plan-Apochromat 63x 1.4 NA Oil DIC M27 immersion lens. Vertices of the cut edges were tracked; the distance of vertex position shifts was measured using Fiji (http://fiji.sc/).

Image processing and automated image analysis

Images were processed and automatically analyzed using custom code in Matlab (KoreTechs), previously described in (Biro et al., 2013). Cell contour detection and classification of cellular regions: segmentation of cells was based on a combination of image filtering, ellipse fitting, and adaptive thresholding. Throughout images and movies, as we are looking at a 2D representation of a 3D cell, of which only the apical surface is exposed, this apical surface in reality constitutes a cortical surface. However within the focused apical plane, the cortex was defined as a region of fixed depth underlying the segmented cell contour. The cytoplasmic region was taken as the difference between the segmented cell area and the cortical region. The definition of the cell contour, cortical and cytoplasmic regions allowed for the extraction of region-specific morphological parameters and intensity values. The effective apical actin concentration was defined as a ratio of mean actin intensity in the cytoplasmic region and mean intensity of actin within cortical region.

Volume measurements

Surface rendering and volume calculations were performed on MCCs expressing UtrCH-GFP, upon embryos immunostaining using anti-GFP antibody and subsequent clearing, with Imarisx64 (Bitplane).